

Surface Morphologies of Langmuir–Blodgett Monolayers of PEO_nPS_n Multiarm Star Copolymers

Ray Gunawidjaja,[†] Sergiy Peleshanko,[†] Kirsten L. Genson,[†] Constantinos Tsitsilianis,[‡] and Vladimir V. Tsukruk^{*,†}

Department of Materials Science and Engineering, Iowa State University, Ames, Iowa 50011, Department of Chemical Engineering, University of Patras, 26504 Patras, Greece, and Institute of Chemical Engineering and High Temperature Chemical Processes, FORTH-ICE/HT, Patras, Greece

Received January 31, 2006. In Final Form: May 3, 2006

Star polymers composed of equal numbers of poly(ethylene oxide) (PEO) and polystyrene (PS) arms with variable lengths and a large (up to 38 total) number of arms, PEO_nPS_n, have been examined for their ability to form domain nanostructures at the air–water and air–solid interfaces. All PEO_nPS_n star polymers formed stable Langmuir–Blodgett (LB) monolayers transferable to a solid substrate. A range of nanoscale surface morphologies have been observed, ranging from cylindrical to circular domains to bicontinuous structures as the weight fraction of the PEO block varied from 19% to 88% and *n* from 8 to 19. For the PS-rich stars and at elevated surface pressure, a two-dimensional supramolecular netlike nanostructure was formed. In contrast, in the PEO-rich star polymer with the highest PEO content, we observed peculiar dendritic superstructures caused by intramolecular segregation of nonspherical core–shell micellar structures. On the basis of Langmuir isotherms and observed monolayer morphologies, three different models of possible surface behavior of the star polymers at the interfaces were proposed.

Introduction

Molecular architecture has been shown to affect the morphology of micellar aggregates of star and star block copolymers in polymer solutions, in the bulk state, and in thin polymer films at the surface and interfaces.^{1,2} The synthesis of block copolymers and the microphase separation of these multicomponent copolymers in bulk³ and sol–gel⁴ states as well as aggregation properties in solution,⁵ at interfaces,⁶ and at surfaces⁷ have been the focus of numerous recent studies. Amphiphilic block copolymers on solid substrates are known to self-organize into well-defined morphologies, as was observed by Zhu et al. for polystyrene-*b*-poly(4-vinylpyridine), PS-*b*-P4VP.⁸ This class of

material possesses crystalline–amorphous interactions in addition to the incompatibility of dissimilar blocks that is responsible for microphase separation.⁹ The combination of amorphous hydrophobic polystyrene (PS) and nonionic and highly crystalline hydrophilic poly(ethylene oxide) (PEO) is among those widely studied. Their high incompatibility leads to well-separated microphase structures. For PEO–PS block copolymers, crystallization of the PEO chains for monolayers at a solid support is frequently suppressed.⁹ In fact, even at 92 wt % PEO phase, microphase separation in the form of very fine dot surface morphology is observed without any sign of crystalline phases.¹⁰ The properties of PEO–PS block copolymers with linear architecture, variable molecular weight, and certain chemical compositions were reported in terms of their bulk behavior,¹¹ phase structures,¹² and morphologies,¹³ as well as their micellar structures in water¹⁴ and organic solvents of different affinities.^{11,15}

Star block copolymers with different blocks confined to a single center qualitatively exhibit behavior similar to linear block copolymers at the air–water interface: hydrophilic chains form a partially submerged pancake structure as the hydrophobic chains collapse into segregated globules.¹⁶ Surface studies performed for PEO–PS block copolymers containing 7, 15.5, 60, and 92 wt % PEO content showed that a sufficient amount of PEO block (greater than 10 wt %) yields uniform dot morphology.¹⁰ Otherwise, spaghetti, islands, or mixed morphologies were formed

* Corresponding author. E-mail: vladimir@iastate.edu.

[†] Iowa State University.

[‡] University of Patras and FORTH-ICE/HT.

(1) (a) Hsieh, H. L.; Quirk, R. P. *Anionic Polymerization: Principles and Practical Applications*; Marcel Dekker: New York, 1996. (b) *Star and Hyperbranched Polymer*; Mishra, M. K., Kobayashi, S., Eds.; Marcel Dekker: New York, 1999. (c) Sperling, L. H. *Introduction to Physical Polymer Science*, 3rd ed.; Wiley-Interscience: New York, 2001. (d) Hadjichristidis, N. *J. Polym. Sci., Part A: Polym. Chem.* **1999**, *37*, 857. (e) Matyjaszewski, K.; Xia, J. *Chem. Rev.* **2001**, *101*, 2921.

(2) (a) Halperin, A.; Tirrell, M.; Lodge, T. P. *Adv. Polym. Sci.* **1992**, *100*, 33. (b) Zhao, B.; Brittain, W. J. *Prog. Polym. Sci.* **2000**, *25*, 677. (c) Koutos, V.; Van der Vegte, E. W.; Hadziioannou, G. *Macromolecules* **1999**, *32*, 1233. (d) Tsukruk, V. V.; Sidorenko, A.; Gorbunov, V. V.; Chizhik, S. A. *Langmuir* **2001**, *17*, 6715. (e) Tsukruk, V. V. *Adv. Mater.* **2001**, *13*, 95. (f) Julthongpipit, D.; Lin, Y.-H.; Teng, J.; Zubarev, E. R.; Tsukruk, V. V. *J. Am. Chem. Soc.* **2003**, *125*, 15912. (g) Green, P. F.; Christensen, T. M.; Russell, T. P.; Jerome, R. *Macromolecules* **1989**, *22*, 2189.

(3) (a) Yang, L.; Hong, S.; Gido, S. P.; Velis, G.; Hadjichristidis, N. *Macromolecules* **2001**, *34*, 9069. (b) Zhu, L.; Huang, P.; Chen, W. Y.; Ge, Q.; Quirk, R. P.; Cheng, S. Z. D.; Thomas, E. L.; Lotz, B.; Hsiao, B. S.; Yeh, F.; Liu, L. *Macromolecules* **2002**, *35*, 3553.

(4) Shen, J.; Zhang, X.; Yin, R. *Macromol. Chem. Macromol. Symp.* **1991**, *46*, 157.

(5) (a) Jeong, U.; Ryu, D. Y.; Kho, D. H.; Lee, D. H.; Kim, J. K.; Russell, T. P. *Macromolecules* **2003**, *36*, 4125. (b) Pispas, S.; Hadjichristidis, N.; Potemkin, I.; Khokhlov, A. *Macromolecules* **2000**, *33*, 1741. (c) Pispas, S.; Poulos, Y.; Hadjichristidis, N. *Macromolecules* **1998**, *31*, 4177.

(6) (a) Nakano, M.; Deguchi, M.; Endo, H.; Matsumoto, K.; Matsuoka, H.; Yamaoka, H. *Macromolecules* **1999**, *32*, 6088. (b) Mahltig, B.; Jérôme, R.; Stamm, M. *Phys. Chem. Chem. Phys.* **2001**, *3*, 4371.

(7) Anastasiadis, S. H.; Retsof, H.; Pispas, S.; Hadjichristidis, N.; Neophytides, S. *Macromolecules* **2003**, *36*, 1994.

(8) Zhu, J.; Eisenberg, A.; Lennox, B. *J. Am. Chem. Soc.* **1991**, *113*, 5583.

(9) Chen, H.-L.; Wu, J.-C.; Lin, T.-L.; Lin, J. S. *Macromolecules* **2001**, *34*, 6936.

(10) Baker, S. M.; Leach, K. A.; Devereaux, C. E.; Gragson, D. E. *Macromolecules* **2000**, *33*, 5432.

(11) Mortensen, K.; Brown, W.; Almdal, K.; Alami, E.; Jada, A. *Langmuir* **1997**, *13*, 3635.

(12) Zhu, L.; Chen, Y.; Zhang, A.; Calhoun, B. H.; Chun, M.; Quirk, R. P.; Cheng, S. Z. D.; Hsiao, B. S.; Yeh, F.; Hashimoto, T. *Phys. Rev. B* **1999**, *60*, 10022.

(13) (a) Zhu, L.; Cheng, S. Z. D.; Calhoun, B. H.; Ge, Q.; Quirk, R. P.; Thomas, E. L.; Hsiao, B. S.; Yeh, F.; Lotz, B. *Polymer* **2001**, *42*, 5829. (b) Reining, B.; Keul, H.; Höcker, H. *Polymer* **2002**, *43*, 7145.

(14) Cogan, K. A.; Gast, A. P. *Macromolecules* **1990**, *23*, 745.

(15) (a) Hiekl, P.; Ballauff, M.; Jada, A. *Macromolecules* **1996**, *29*, 4006. (b) Yu, K.; Eisenberg, A. *Macromolecules* **1996**, *29*, 6359. (c) Seo, Y.; Kim, M.; Ou-Yang, D.; Peiffer, D. *Polymer* **2002**, *43*, 5629.

Table 1. Molecular Characteristics of PEO_nPS_n Heteroarm Star Polymers

group	sample	composition	no. of arms		PS		PEO		ϕ_{PEO}	M_w total
			N	total	M_w	N_{PS}	M_w	N_{PEO}		
I	S16-19	PEO ₈ -PS ₈	8	16	27 000	260	5 600	127	0.19	241 000
	S18-23	PEO ₉ -PS ₉	9	18	22 000	212	6 500	148	0.23	245 000
	S16-39	PEO ₈ -PS ₈	8	16	15 000	144	9 100	207	0.39	185 500
II	S38-78	PEO ₁₉ -PS ₁₉	19	38	3 000	29	14 200	323	0.78	339 000
	S30-86	PEO ₁₅ -PS ₁₅	15	30	3 000	29	22 500	511	0.86	393 000
	S20-88	PEO ₁₀ -PS ₁₀	10	20	3 100	30	25 000	568	0.88	284 000
	L-86	PEO-PS	1	2	3 200	31	20 400	464	0.86	23 600

depending on the deposition and spreading conditions.¹⁷ A similar trend was observed for PEO-PS_n asymmetrical heteroarm star polymers studied in our group,¹⁸ as well as symmetrical PS-*b*-PEO and PB-*b*-PEO star block copolymers studied by Duran's group.¹⁶ A rather unusual morphology was reported for PS₆-*s*-poly(acrylic acid)₆ (PS₆-*s*-PAA₆) star copolymer with two-dimensional circular micelles forming as a result of the rigid disk-like aromatic core and short polymer chains.¹⁹

The A_nB_n star copolymers possess the ability to self-assemble under appropriate conditions. In dilute solutions and in a solvent selective for one type of arm, the heteroarm star polymers form unimolecular micelles at relative moderate concentrations as their architecture can mimic a micellar structure.^{20a,b} At concentrations above the critical micelle concentration (cmc) (which can be 3 orders of magnitude higher than that of the linear counterparts), they are associated into polymolecular micelles with low aggregation number, adopting a core-shell spherical structure.^{20c} At elevated concentrations in water-oil mixtures, PEO₁₀PS₁₀ self-assembles to form a hexagonal lyotropic liquid crystalline structure comprised of cylindrical arrays where the divinylbenzene (DVB) cores of the stars are located on the polar/nonpolar interface (i.e., on the surface of the cylinders), the PS arms are segregated on the interior of the cylinders, and the PEO arms are located in the aqueous polar external domains.^{20d}

Recent studies have demonstrated that branched PEO-PS star polymers might form unique morphologies not observed for linear block copolymers with peculiar properties.²¹ For example, the aggregation number is usually lower for star copolymers because of the crowding of polymeric chains at a single junction point that hinders aggregation of PS blocks.¹⁸ However, the

number of arms in amphiphilic star polymers studied to date is usually very limited and does not exceed six.²¹ The effect of a high number of dissimilar arms (>10) attached to a single core on the phase state and morphology of heteroarm star polymers remains unknown. Therefore, to consider the role of the crowding of the hydrophilic and hydrophobic chains attached to a single core in their surface behavior and morphology, we exploit a series of PEO_nPS_n star polymers with a large number of arms (2*n* up to 38) and with a PEO content, ϕ (wt %), ranging from 19 to 88% (Figure 1, Table 1).

Experimental Section

The PEO_nPS_n heteroarm star polymers have been synthesized via three-step sequential anionic polymerization under inert atmosphere, as described elsewhere.²² The molecular weight, polydispersity, and architectures were verified using the combination of gel permeation chromatography (GPC), ¹H NMR, and light scattering, as summarized in Table 1.²² For further discussion, the notation *S**m*- ϕ will be used to refer to the polymers studied here, where *m* is the total number (*m* = 2*n*) of arms and ϕ is PEO content (wt %) (Table 1).

Langmuir isotherms at the air-water interface and Langmuir-Blodgett (LB) deposition onto a silicon substrate were conducted at room temperature using a KSV 2000 LB minitrough according to the usual procedure.²³ A 60–120 μ L volume of dilute polymer solution (concentration less than 0.5 mg/mL) in chloroform (HPLC grade) was deposited in 5–10 drops uniformly distributed onto the water surface (Nanopure, 18.0 M Ω cm) and left to evaporate and spread evenly over a period of 30 min. Surface molecular area *A*₁ was calculated as the point of initial appearance of the rising surface pressure (>0.1 mN/m). The limiting cross-sectional area *A*₀ was determined at the steep rise in the surface pressure related to the formation of condensed monolayer. Highly polished [100] silicon wafers (Semiconductor Processing Co.) were cut into rectangular pieces (2 × 2 cm²) and sonicated in Nanopure water for 10 min to remove silicon dust. The wafers were then chemically treated with "piranha solution" (30% concentrated hydrogen peroxide, 70% concentrated sulfuric acid, *hazardous solution!*) for 1 h to remove organic and inorganic contaminants and to strip the original silicon oxide surface layer.²⁴ Finally, wafers were abundantly rinsed with Nanopure water and dried with dry nitrogen. During LB deposition,

(16) (a) Francis, R.; Taton, D.; Logan, J. L.; Masse, P.; Gnanou, Y.; Duran, R. S. *Macromolecules* **2003**, *36*, 8253. (b) Francis, R.; Skolnik, A. M.; Carino, S. R.; Logan, J. L.; Underhill, R. S.; Angot, S.; Taton, D.; Gnanou, Y.; Duran, R. S. *Macromolecules* **2002**, *35*, 6483. (c) Logan, J. L.; Masse, P.; Dorvel, B.; Skolnik, A. M.; Sheiko, S. S.; Francis, R.; Taton, D.; Gnanou, Y.; Duran, R. S. *Langmuir* **2005**, *21*, 3424. (d) Logan, J. L.; Masse, P.; Gnanou, Y.; Taton, D.; Duran, R. S. *Langmuir* **2005**, *21*, 7380. (e) Matmour, R.; Francis, R.; Duran, R. S.; Gnanou, Y. *Macromolecules* **2005**, *38*, 7754.

(17) (a) Devreaux, C. A.; Baker, S. M. *Macromolecules* **2002**, *35*, 1921. (b) Cheyne, R. B.; Moffitt, M. G. *Langmuir* **2005**, *21*, 5453.

(18) (a) Peleshanko, S.; Gunawidjaja, R.; Jeong, J.; Shevchenko, V. V.; Tsukruk, V. V. *Langmuir* **2004**, *20*, 9423. (b) Peleshanko, S.; Jeong, J.; Gunawidjaja, R.; Tsukruk, V. V. *Macromolecules* **2004**, *37*, 6511.

(19) Genson, K. L.; Hoffman, J.; Teng, J.; Zubarev, E. R.; Vaknin, D.; Tsukruk, V. V. *Langmuir* **2004**, *20*, 9044.

(20) (a) Gorodyska, A.; Kiriy, A.; Minko, S.; Tsitsilianis, C.; Stamm, M. *Nano Lett.* **2003**, *3*, 365. (b) Kiriy, A.; Gorodyska, G.; Minko, S.; Stamm, M.; Tsitsilianis, C. *Macromolecules* **2003**, *36*, 8704. (c) Voulgaris, D.; Tsitsilianis, C.; Esselink, F.; Hadziioannou, G. *Polymer* **1998**, *39*, 6429. (d) Tsitsilianis, C.; Alexandridis, P.; Lindman, B. *Macromolecules* **2001**, *34*, 5979.

(21) (a) Herman, D. S.; Kinning, D. J.; Thomas, E. L.; Fetters, L. J. *Macromolecules* **1987**, *20*, 2940. (b) Tselikas, Y.; Hadjichristidis, N.; Lescanec, R. L.; Honeker, C. C.; Wohlgemuth, M.; Thomas, E. L. *Macromolecules* **1996**, *29*, 2290. (c) Pochan, D. J.; Gido, S. P.; Pispas, S.; Mays, J. W.; Ryan, A. J.; Fairclough, P. A.; Hamley, I. W.; Terrill, N. J. *Macromolecules* **1996**, *29*, 5091. (d) Lin, Y.-H.; Teng, J.; Zubarev, E. R.; Shulha, H.; Tsukruk, V. V. *Nano Lett.* **2005**, *5*, 491. (e) Pochan, D. J.; Gido, S. P.; Pispas, S.; Mays, J. W. *Macromolecules* **1996**, *29*, 5099. (f) Grayer, V.; Dormidontova, E.; Hadziioannou, G.; Tsitsilianis, C. *Macromolecules* **2000**, *33*, 6330. (g) Wert, M. P. L.; Van der Vegte, E. W.; Grayer, V.; Esselink, E.; Tsitsilianis, C.; Hadziioannou, G. *Adv. Mater.* **1998**, *10*, 452.

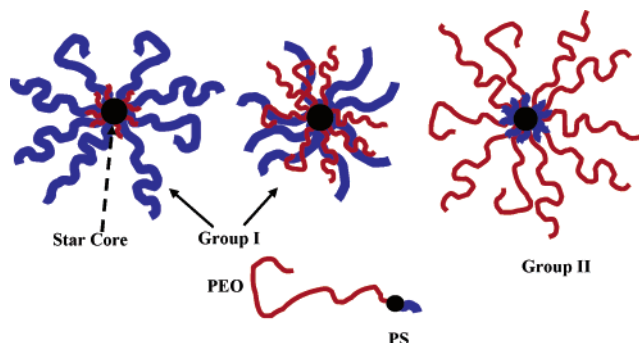


Figure 1. Schematics of PEO_nPS_n heteroarm star polymers with larger number of arms and low (left), moderate (center), and high (right) PEO contents. Schematic of linear block copolymer molecule is shown as well.

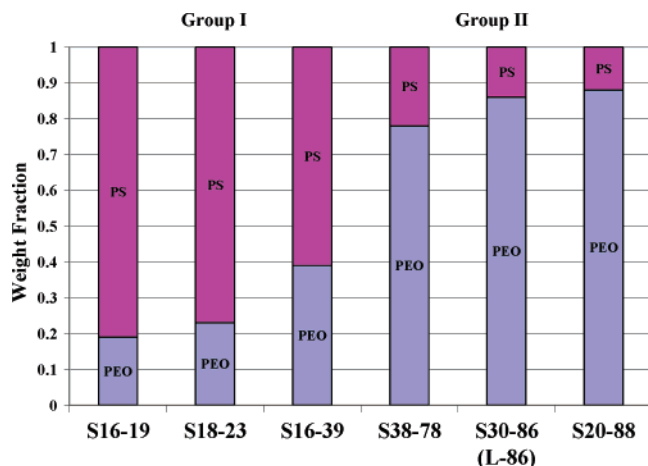


Figure 2. Graphic representation of the weight fraction of the PEO and PS blocks for PEO_nPS_n heteroarm star polymers.

the surface pressure was held constant as the submerged substrate was slowly lifted from the trough at a rate of 3 mm/min.

The effective thickness of the LB monolayers was measured with a COMPEL automatic ellipsometer (InOmTech, Inc.) at an incident angle of 70° and a wavelength of 634 nm according to the well-known experimental procedure.²⁵ The LB monolayers on the silicon substrates were studied with a Dimension-3000 atomic force microscope (AFM) in the “light” tapping mode in accordance with the usual procedure adapted in our laboratory.²⁶ An amplitude ratio of 0.95 and higher was employed to avoid monolayer damage.²⁷ AFM characterization of the deposited LB monolayers was done after drying in a desiccator for 24 h. The AFM scans were conducted at 1 Hz scanning rate for surface areas ranging from $50 \times 50 \mu\text{m}^2$ to $1 \times 1 \mu\text{m}^2$ and for several randomly selected locations with at least 40 different images collected for each specimen. The domain heights were obtained from the cross-sectional analysis of monolayer topography, and the PS domain surface area coverage was calculated from height histograms using the bearing analysis.²⁸ The AFM tip radii were between 20 and 35 nm, and the spring constants of these cantilevers were in the range of 40–60 N/m. The tip radius was measured independently using tethered gold nanoparticles as a standard reference, and only the sharpest tips were selected for high-resolution scanning.

Results and Discussion

Six star copolymers studied here are composed of an equal number of PEO and PS arms attached to a central core (Figure 1). The weight content of the PEO blocks varied from 19% to 88% as the number of arms varied from eight arms of PEO and PS each for S16-19 to 19 arms of PEO and PS each for S38-78 (Table 1, Figure 2). All arms of the same nature have the same molecular weight. An example of a linear diblock copolymer was included for one particular composition for comparative purposes (L-86, Table 1). For clarity, we consider all compounds studied here in two groups: group I with lower PEO content (<50%) and group II with a predominant PEO content (79–88%) (Figures 1 and 2). Within the first group, the total number of arms was close (16–18), although within the second group

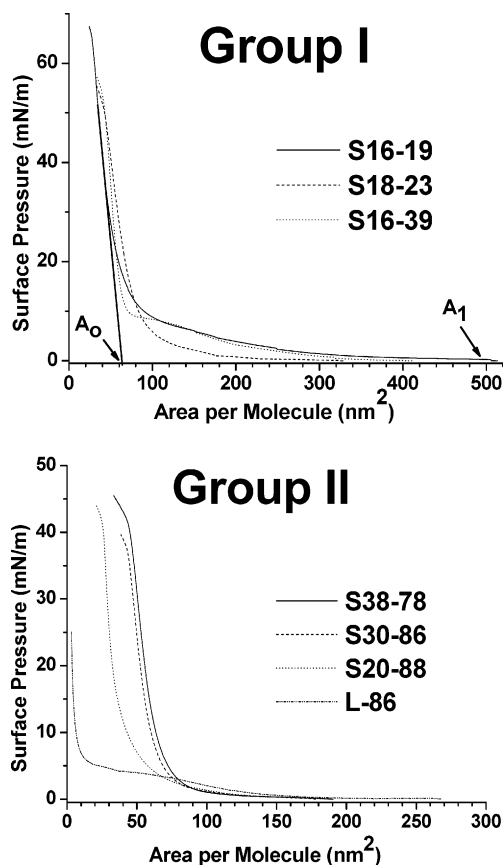


Figure 3. Langmuir isotherms of PEO_nPS_n star polymers with low PEO content, S16-19, S18-23, and S16-39 (top); and high PEO content, S38-78, S30-86, and S20-88 (bottom).

the number of arms increased up to 38 for star copolymers with lower PEO content (Table 1).

Surface Behavior at the Air–Water Interface. All heteroarm star polymers studied here formed stable Langmuir monolayers at the air–water interface, indicating proper amphiphilic balance of the molecular architectures (see π – A isotherms in Figure 3). The reversibility of the Langmuir monolayers was examined by repeating cycles of compression and expansion within the low-pressure (<5 mN/m) regime. The star copolymers S38-78, S30-86, and S20-88 showed a very small hysteresis (5–10% surface area) after a period of relaxation (10 min). A slightly larger hysteresis (10–15% surface area) observed for star copolymers S16-19, S18-23, and S16-39 indicated partially irreversible behavior due to the presence of a larger fraction of glassy PS phase aggregated at high surface pressure.

The heteroarm star polymers from group I with a larger PS content exhibited higher initial surface molecular areas and a low-pressure plateau on isotherms (Figure 3, top, and Table 2). The star copolymers from group II displayed much smaller initial cross-sectional areas (several times) and a more gradual transition in the surface pressure on the isotherms with no plateau prior to the steep increase in the surface pressure before monolayer collapse (Figure 3, bottom, and Table 2). The lower PS content (corresponding to the shorter length of PS chains, Table 1) translated into a reduced initial surface molecular area, A_1 , and limiting cross-sectional area, A_0 (Table 2).

To establish a contribution of the PS and PEO chains into A_1 and A_0 areas, we estimated the theoretical limiting surface areas per molecule using different models of chain conformations. In the first model, we considered a situation when PS and PEO chains in coiled conformation are the limiting factors in monolayer

(22) Tsitsilianis, C.; Papanagopoulos, D.; Lutz, P. *Polymer* **1995**, *36*, 3745.

(23) Ulman, A. *An Introduction to Ultrathin Organic Films: From Langmuir-Blodgett to Self-Assembly*; Academic Press: Boston, MA, 1991.

(24) Tsukruk, V. V.; Bliznyuk, V. N. *Langmuir* **1998**, *14*, 446.

(25) Azzam, R. M. A.; Bashara, N. M. *Ellipsometry and Polarized Light*; North-Holland: New York, 1977.

(26) (a) Tsukruk, V. V.; Reneker, D. H. *Polymer* **1995**, *36*, 1791. (b) Tsukruk, V. V. *Rubber Chem. Technol.* **1997**, *70*, 430.

(27) Magonov, S. N.; Elings, V.; Whangbo, M.-H. *Surf. Sci.* **1997**, *375*, L385.

(28) Magonov, S. N. *Surface Analysis with STM and AFM: experimental and theoretical aspects of image analysis*; VCH: New York, 1996.

Table 2. Experimental and Calculated Surface Areas per Molecule of Amphiphilic PEO_nPS_n Star Polymers

group	sample	$R_g(\text{core}),^b$ nm	area per molecule, nm ² /molecule							
			experimental		calculated					
			A_o	A_1	random coil ^a		LS data ^b		star shape ^c	
				A'_{PS}	A'_{PEO}	A''_{PS}	A''_{PEO}	A'''_{PS}	A'''_{PEO}	
I	S16-19	1.2	70	500	130	290	448	134	534	220
	S18-23	1.6	81	320	123	381	391	171	489	292
	S16-39	1.2	68	380	74	468	249	209	300	346
II	S38-78	1.9	66	192	44	1728	78	363	123	665
	S30-86	1.5	62	180	33	2155	67	525	99	953
	S20-88	1.1	40	185	22	1595	57	548	76	962
	L-86		8	165	2	130	8	91	11	214

^a This model used limited areas of the PS (0.06 nm²) and PEO (0.28 nm²) monomeric units.^{18b} ^b Parameters were calculated using experimental data for the star polymers in solution ($K = 0.044$ and $a = 0.706$).²² ^c This model employed the molecular conformation with branching parameters.^{31,32}

compression. We calculated the surface area per molecule for total individual PS and PEO chains from the known limiting surface area for PS (0.06 nm²) and PEO (0.28 nm²) monomeric unit reported for PEO–PS linear²⁹ and star polymers^{18b} with a limited numbers of arms deposited at the air–water interface (Table 2). Theoretical surface area per molecule A' was calculated from the surface area per monomer, a_o , number of monomers in a single arm, N , and number of arms, n : $A' = a_o N n$ (Table 2).

The theoretical surface area per molecule A'' was alternatively calculated using light scattering (LS), assuming PS and PEO chains in coiled conformation in good solvent (second model) (Table 2). Considering tetrahydrofuran (THF) and chloroform are both nonselective solvents with comparable properties,³⁰ for coil dimensions we applied the Mark–Houwink–Sakurada (MHS) equation by using LS data described earlier for these star polymers.²² We assumed that MHS constants K and a found for S18-23 and S16-39 are the same for all PEO_nPS_n heteroarm star polymers (Table 2).

The third model included corrections for the branching introduced by Stockmayer and Zimm³¹ and later modified by Birshtein and Zhulina to describe the conformation of the star polymers in θ -solvent. The radius of gyration R_g for both PS and PEO chains in a random coil conformation was calculated according to³²

$$R_g = [\sqrt{(3n-2)/n}](r/\sqrt{6})$$

The end-to-end distance r for this model was calculated as described in the literature: $r = a N_k^{3/5}$.^{18b,33} a is the segment length (Kuhn segment), and N_k is the number of segments: $N_k = N/n_s$, where n_s is the number of monomer units in one Kuhn segment and N is the number of monomer units in the polymer chain. The literature data are used for two blocks: for PS, $a = 1.69$ nm and $n_s = 6$; for PEO, $a = 0.77$ nm and $n_s = 2$.³⁴ The total radius of a star polymer is $R_t = 2R_g + R_c$, where R_c is a radius of a core. Apparently, the random coil approximation did not account for the effect of the multiarm star architecture, but models based on LS data and branching parameter (star shape)

assumed conformation of the star polymers in nonselective solvent and θ -solvent, respectively, with all arms stretched out of a central core.

All molecular area data were corrected by adding an area per molecule occupied by the core as presented in Table 2. R_c of the core was calculated based on the mole ratio, v , of divinylbenzene (DVB) to living PS ends:

$$R_c = \sqrt[3]{(3V_c)/(4\pi)}$$

where V_c is the core's molar volume.²² The molar volume of DVB core was calculated as follows:

$$V_c = (M_{n(\text{DVB})} n v) / (N_a d)$$

where M_n is the molar weight of DVB (0.1302 kg/mol), N_a is Avogadro's number, and d is the density of the DVB core assumed to be equal to the density of bulk PS (1060 kg/m³).³⁵

The theoretical surface areas per molecules estimated from chemical composition under different scenarios and the experimental surface area as measured in the condensed state of Langmuir monolayer show similar trends (Figure 4). Dashed lines correspond to the ideal calculations when experimental data agree with theoretical values. For all star copolymers, the experimental area per molecule A_o , corresponding to the collapsed PS chains, is similar (ca. 70 nm²) (Figure 4). Significant differences in theoretical and observed values of A_o for the star polymers of group I could correspond to the collapsed PS arms extensively stretched out of the air–water interface, which drastically reduce the limiting surface areas for the PS monomeric unit (Table 2 and Figure 4, top). On the contrary, small differences in theoretical (A''_{PS} and A'''_{PS} , Table 2 and Figure 4, bottom) and experimental values of A_o for the star polymers of group II allowed us to suggest that their PS chains stayed mostly stretched out of a core along the air–water interface upon compression.

Comparison of the experimental initial surface molecular area A_1 with theoretical values of A_{PS} and A_{PEO} calculated for all three models led us to following conclusions. The PS chains of the S16-19 and S18-23 star polymers mostly account for its initial surface molecular area, A_1 (Table 2). This observation can be due to increased length of the PS arms which reduced its mobility, influentially long PEO chains, and an effect of the crowding in the arms that together forced multiple PS arms to remain expanded and spread in lateral directions rather than stretching out of the interface. However, for group II, the area per molecule A_1 mostly depended on the length of the PEO chains. The surface areas per

(29) (a) Cox, J. K.; Yu, K.; Constantine, B.; Eisenberg, A.; Lennox, R. B. *Langmuir* **1999**, *15*, 7714. (b) Kawaguchi, M.; Sauer, B. B.; Yu, H. *Macromolecules* **1989**, *22*, 1735. (c) Kumaki, J. *Macromolecules* **1988**, *21*, 749.

(30) Erhardt, R.; Boker, A.; Zettl, H.; Kaya, H.; Pyckhout-Hintzen, W.; Krausch, G.; Abetz, V.; Muller, A. H. E. *Macromolecules* **2001**, *34*, 1069.

(31) Stockmayer, W. H.; Zimm, B. H. *J. Chem. Phys.* **1949**, *17*, 1301.

(32) Birshtein, T. M.; Zhulina, E. B. *Polymer* **1984**, *25*, 1453.

(33) Sperling, L. H. *Introduction to physical polymer science*; Wiley-Interscience: New York, 1986.

(34) Aharoni, S. M. *Macromolecules* **1983**, *16*, 1722.

(35) Wunderlich, B. *Macromolecular physics*; Academic Press: New York, 1973; Vol. 1.

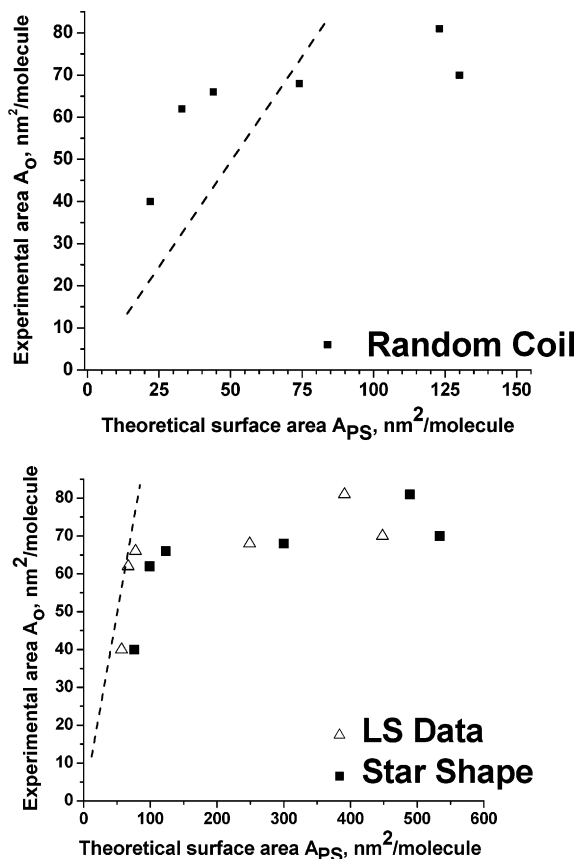


Figure 4. Comparison of experimental A_o and theoretical (A_{PS}) molecular surface area for different conformational models. Dashed line shows correlation between experimental and theoretical values.

molecule A_1 values were drastically lower than theoretical values of A_{PEO} due to a large number of arms (up to 38), which can cause considerable steric difficulties for the PEO chains to arrange at the interface. Therefore, we can suggest that, for the PEO_nPS_n amphiphilic star copolymers, PEO arms surround the PS core forming an intermediate dense PEO layer to protect it from water subphase and, as a result, only partially stretch out from the collapsed core. This would cause significantly lower values of A_1 of the star copolymers, which has been observed, especially for the polymers of group II. A similar phenomenon was observed earlier for the polystyrene–poly(2-vinylpyridine) (PS_6P2VP_6) heteroarm star polymers in toluene.³⁶ Analysis of the LS data for these polymers revealed that the corona composed from PS chains was located closer to the core to protect the insoluble parts of the micelles. This model was confirmed by computational simulations of the heteroarm star polymers behavior in good and selective solvents.³⁷

Although S16-39 star polymer belongs to group I, it had an unusually high A_1 value due to an increasing content of the PEO block (see Table 1). Comparison of all calculated models revealed that the random coil model (involving the limiting surface areas for both monomeric units) demonstrated the best agreement between experimental values of A_o and A_1 and theoretical values of A_{PS} and A_{PEO} , respectively. Thus, PEO and PS chains of the S16-39 heteroarm star polymer are mostly phase separated at the air–water interface, forming Janus structures, which have two different sections of opposite philicity: hydrophilic PEO and hydrophobic PS.

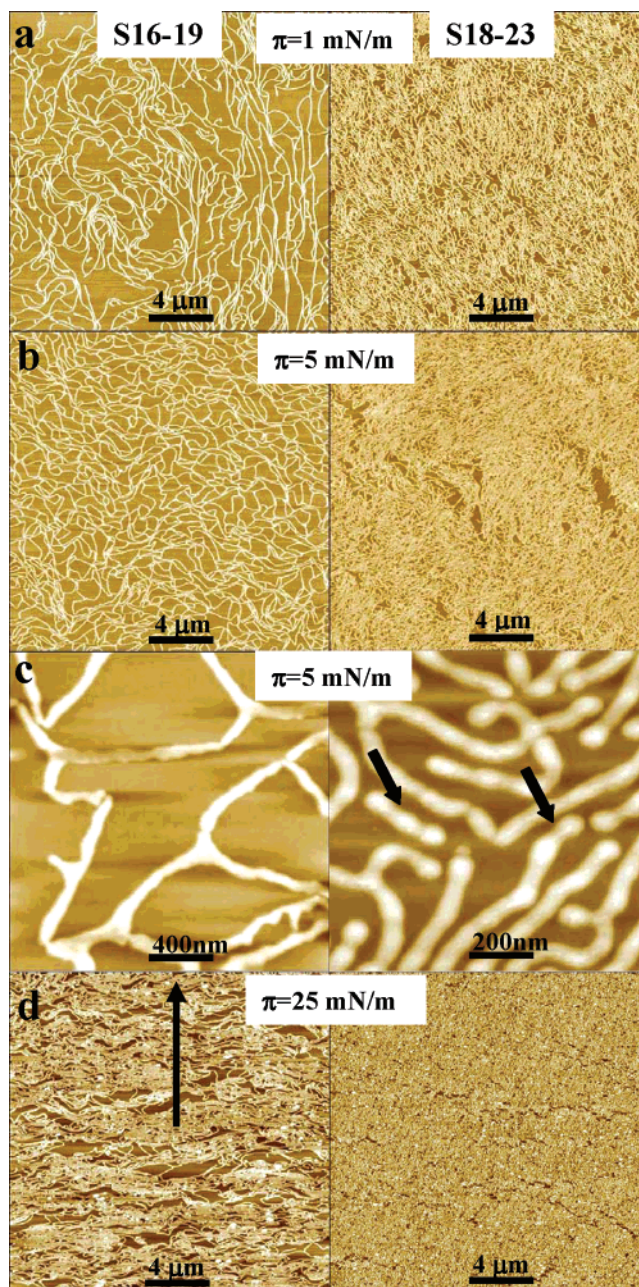


Figure 5. Cylindrical structures of LB monolayers from heteroarm star polymers with the lowest PEO content S16-19 (left) and S18-23 (right) deposited at 1 (a), 5 (b and c) and 25 mN/m (d). Height is 15 nm for all images. Arrow (image d) indicates the dipping direction.

LB Monolayers at the Solid Surface: Group I. The role of the number of arms and the weight fraction of the polymeric blocks on surface domain morphology was elucidated with AFM imaging. Two heteroarm star polymers with the lowest PEO content (group I) formed cylindrical domains with random orientation and a low degree of branching (Figure 5). The continuous cylindrical domains of S16-19 had moderate height (6.8 ± 0.2 nm) and apparent width (180 ± 40 nm) (Table 3). The cylindrical domains were randomly looped, covering approximately a quarter of the substrate surface at lower surface pressure. At higher pressure, the surface coverage increased to 66% as the height increased to 9.0 nm (Figure 5d, left). The cylindrical domains at the highest surface pressure became oriented in the dip direction, suggesting that the microscopic ordering is controlled by the capillary forces in the course of LB deposition.

(36) Voulgaris, D.; Tsitsilianis, C.; Grayer, V.; Esselink, F. J.; Hadziioannou, G. *Polymer* **1999**, *40*, 5879.

(37) Havránková, J.; Limpouchová, Z.; Procházka, K. *Macromol. Theory Simul.* **2003**, *12*, 512.

Table 3. Characteristics of LB Monolayers of PEO_nPS_n Star Polymers at Different Pressures (π , mN/m)

group	sample	thickness, nm			domain height, nm			area coverage		
		$\pi = 1$	$\pi = 5$	$\pi = 25$	$\pi = 1$	$\pi = 5$	$\pi = 25$	$\pi = 1$	$\pi = 5$	$\pi = 25$
I	S16-19	1.1	1.4	2.7	7.0	6.6	9.0	0.24	0.29	0.66
	S18-23	2.1	2.2	3.6	5.5	5.4	6.7	0.44	0.64	0.77
	S16-39	1.0	1.8	2.7	3.3	3.6	3.4	0.36	0.63	0.93
II	S38-78	0.8	2.4	3.4	1.5	2.5	1.1	0.57	0.74	0.97
	S30-86	2.4	2.8	4.3	1.2	2.6	2.3	0.59	0.94	1.00
	S20-88	2.6	4.7	7.3	8.1	9.5	9.6	0.29	0.49	0.97
	L-86	0.5	0.4	6.1	0.9	0.9	1.2	NA	NA	NA

The S18-23 star copolymer with more PS and PEO arms and slightly longer PEO arms formed densely packed cylindrical domains (Figure 5, right column). The cylinder height and width were lower than those for previous S16-19 star polymer at all surface pressures (Table 3). In contrast, the effective thickness of the LB monolayer for S18-23 was higher (2.1 ± 0.2 nm, at low surface pressure). This was accompanied by an increase in the surface coverage (44% at lowest surface pressure, 77% at highest surface pressure). Higher resolution AFM imaging revealed fine circular substructures of the cylindrical domains for both star polymers (arrows, Figure 5c). This confirms that the predominant type of aggregation for star copolymers with the lowest PS content is circular domains, as expected for a given chemical composition in the bulk state. However, unlike heteroarm star polymers with a limited number of arms (<6),¹⁸ further aggregation of circular domains into continuous and branched cylindrical domains occurs within the monolayer of star copolymers with a large number of arms (32 and 36 arms). A similar morphological transition from circular to branched cylindrical, more stringlike, domains was observed for star block copolymers upon compression.^{16c,e} However, increasing surface pressure caused a collapse of string domains into large circular domains, which is quite the opposite of the high lateral stability of the cylindrical domains of the heteroarm star polymers studied here.

In some surface areas close to the edges of the LB films, a hierarchical self-organization of the S16-19 and S18-23 heteroarm star copolymers has been revealed (Figure 6). An internal segregation of the different arms is likely to occur at the air-water interface (i.e., PEO in water, PS in air), leading to stable Janus unimolecular micelles of spherical morphology (top arrow, Figure 6a). At higher surface pressure, a second level of organization occurred which included larger circular structures (multimolecular micelles of low aggregation number as expected (bottom arrow, Figure 6a)). These micelles became the building blocks, forming wormlike cylindrical structures (Figure 6a). A similar aggregation has been observed for the S18-23 heteroarm star polymer at moderate surface pressure (5 mN/m), where spheres coexisted with cylinders and other morphologies (Figure 6b). Some very interesting morphologies (i.e., Y-junctions, circular cylinders, and cylinders + circular structures, Figure 6a,b) have been found, resembling those observed by Bates for PB-PEO diblocks in solution.³⁸ To the best of our knowledge, this is the first confirmation of Bates's findings for star copolymers. The ability of the symmetrical heteroarm polymers to form unimolecular and polymolecular micelles has been shown by Voulgaris et al.^{20c,36} In this study, the PS₆P2VP₆ star molecules were observed to associate in polymolecular micelles in toluene. Recent computational models of the heteroarm star polymers showed that appropriate conditions of block compatibility or selective solvents can lead to intramolecular segregation.^{37,39,40}

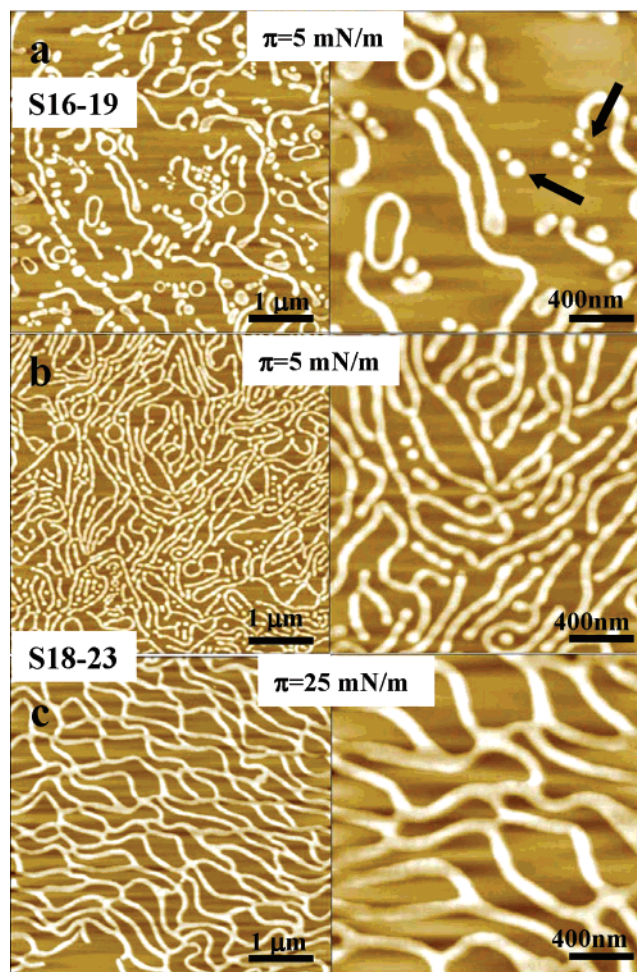


Figure 6. Diverse morphologies at the edges of LB monolayers from S16-19 (a) and S18-23 (b and c) deposited at 5 (a and b) and 25 mN/m (c). Height is 15 nm for all images.

Finally, at high surface pressure a nearly defect-free supramolecular netlike structure has been observed (Figure 6c). A similar pattern has been observed for the LB films of P2VP- and PEO-containing polymers. In the case when P2VP-containing polymers have been used, either another diblock copolymer (PS-*b*-FS)⁴¹ or surfactant molecules (3-pentadecylphenol)⁴² along with solvent-assisted procedure have been utilized to initiate the formation of the nanostrand network. Similar interconnected spaghetti-like patterns of LB films have been examined as one of a few characteristic (but not a prime morphology) features for the asymmetric PS-PEO diblock¹⁷ and heteroarm star polymers.^{18b} By contrast, this kind of peculiar surface morphology seems to be predominant for the PEO_nPS_n heteroarm star polymers at elevated surface pressure.

(38) Jain, S. T.; Bates, F. S. *Science* **2003**, *300*, 460.

(39) Chang, Y.; Chen, W.-C.; Sheng, Y.-J.; Jiang, S.; Tsao, H.-K. *Macromolecules* **2005**, *38*, 6201.

(40) Vanakaras, A. G. *Langmuir* **2006**, *22*, 88.

(41) Seo, Y.-S.; Kim, K. S.; Galambos, A.; Lammertink, R. G. H.; Vancso, G. J.; Sokolov, J.; Rafailovich, M. *Nano Lett.* **2004**, *4*, 483.

(42) Lu, Q.; Bazuin, C. G. *Nano Lett.* **2005**, *5*, 1309.

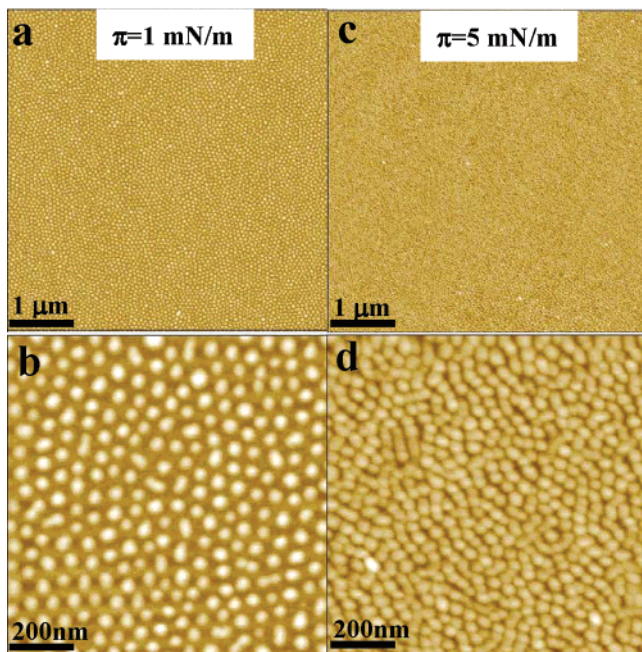


Figure 7. AFM images of LB monolayers from star polymer with moderate content of PEO (S16-39) at 1 (a and b) and 5 mN/m (c and d). Height is 10 nm for all images.

The star copolymer with a moderate PEO content (S16-39) stands alone in group I (Table 1, Figure 2). Unlike the other two group I copolymers, S16-39 formed a very uniform monolayer at both low and high surface pressures (Figure 7a,c). Fine circular domains formed a densely packed and partially ordered network visible at higher resolution (Figure 7b,d). The network possesses a short-range ordering of PS domains 3.5 nm high, as can be concluded from two-dimensional fast Fourier transform and lattice cross sections (not shown). The diameter of very uniform circular domains was close to that observed for other polymers (60 ± 5 nm). The domain height remained relatively constant as the surface pressure increased, thereby causing the effective thickness of the monolayers to climb (Table 3). The formation of a relatively ordered lattice in this specimen can be explained by a significantly low PS content combined with a lower overall molecular weight and the molecular weight of PS arms, which results in higher mobility of the molecules, thus facilitating formation of a more ordered lattice of circular domains.

Two-dimensional (2D) Janus-like structures can have either circular or noncircular shapes depending upon the length of the different polymer segments and the number of arms.^{39,40} The Janus structures can facilitate further formation of multimolecular micelles, which indeed was observed for all PEO_nPS_n heteroarm star polymers studied here. Hence, we suggest that a significant difference between PEO and PS chains length in S16-19 and S18-23 star polymers caused noncircular structures, which later assemble themselves into cylindrical micelles. Recent theoretical calculations have shown that, for a 2D system of particles consisting of a hard core and soft repulsive corona, repulsive interactions may cause spontaneous formation of the stripe morphology resembling those observed in this study.⁴³ In the case of S16-39 star polymer, formed spherical Janus particles are organized into ordered supramolecular structures.

LB Monolayers at the Solid Surface: Group II. In contrast with group I, the heteroarm star polymers with the larger number of arms, higher molecular weight, and higher content of PEO

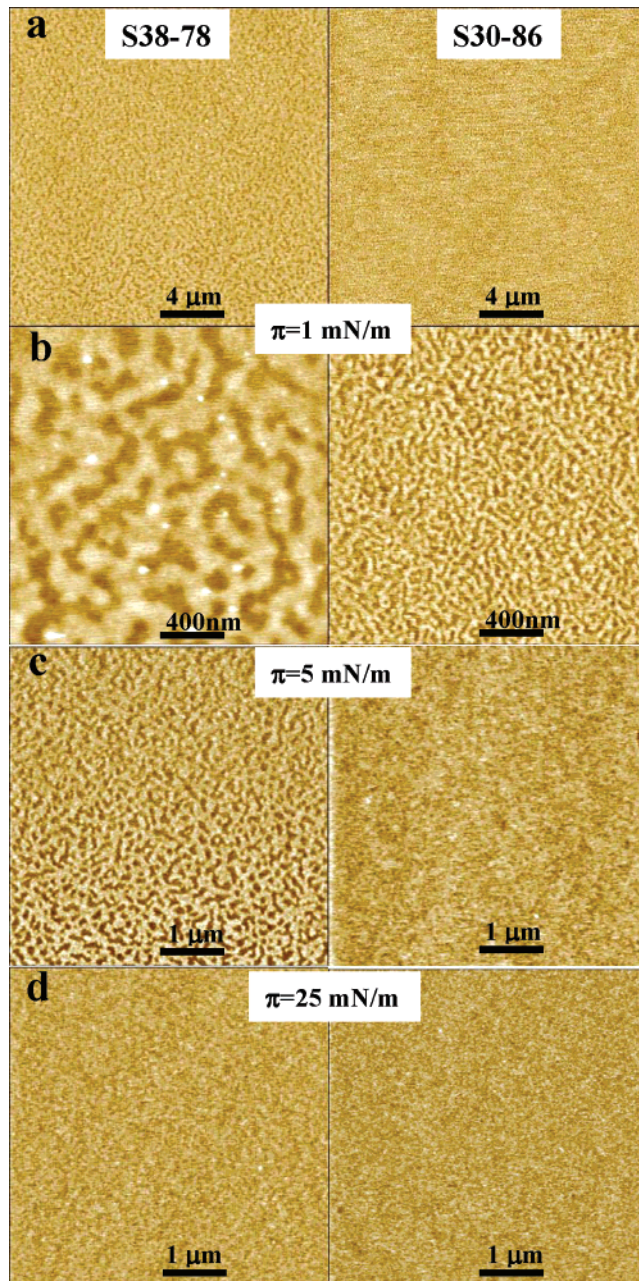


Figure 8. AFM images of LB monolayers from: S38-78 (left) and S30-86 (right) deposited at 1 (a and b), 5 (c), and 25 mN/m (d) surface pressures. Height is 3 nm for all images of S38-78 star polymer (left column) and 5 nm for all images of S30-86 star polymer (right column).

chains formed monolayers with bicontinuous PEO and PS phases (Figure 8). The S38-78 star copolymer with 38 arms formed a uniform monolayer with a fine texture: a bicontinuous network at low surface pressure and dense packing of circular domains as the surface pressure increased. However, the S30-86 heteroarm star polymer formed a coarser network of PS domains at low surface pressure and a uniform monolayer at 25 mN/m (Figure 8c,d). The uniform surface morphology of these star copolymers is similar to the morphology of the linear block copolymer L-86 with identical content of PEO phase (not shown). However, the overall thickness of the monolayer from the linear block copolymer at low surface pressure was much smaller than that for the analogous star copolymer (Table 3). This difference indicates that the presence of the spatial constraints of the multiple arms attached to a single core facilitates easier vertical phase separation under lateral compression. Moreover, the effective

(43) (a) Malescio, G.; Pellicane, G. *Nat. Mater.* **2003**, *2*, 97. (b) Malescio, G.; Pellicane, G. *Phys. Rev. E* **2004**, *70*, 021202.

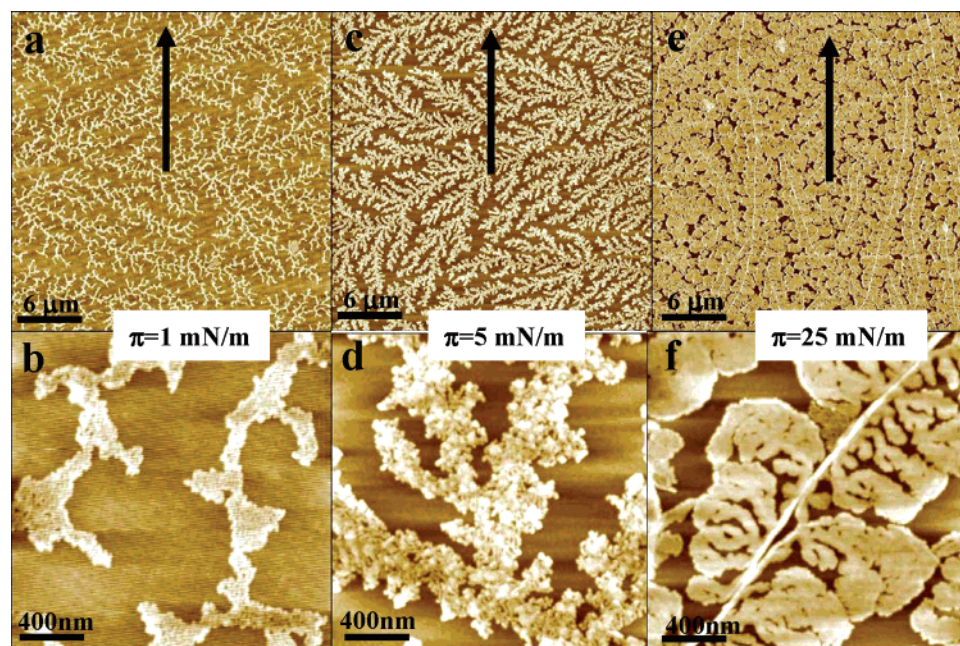


Figure 9. AFM images of dendritic supramolecular nanostructures in LB monolayers from S20-88 at 1 (a, b), 5 (c, d), and 25 mN/m (e, f). Height is 15 nm for all images. Arrows (images a, c, e) indicate the dipping direction.

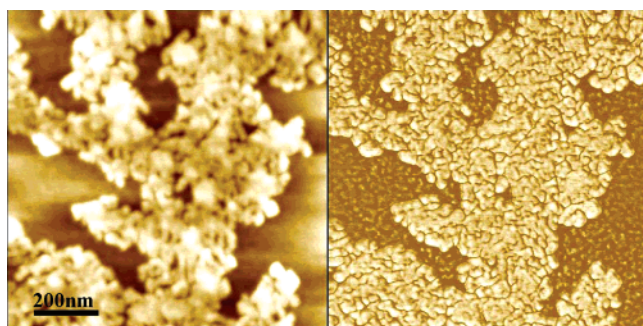


Figure 10. High-resolution AFM images of dendritic structures in LB monolayers from S20-88 at 5 mN/m. Height (left) is 15 nm; phase (right) is 25°.

thickness of LB monolayers increased significantly for higher surface pressure, indicating that the PEO phase formed a thicker layer underneath the PS blocks, ultimately allowing the PS phase to form the uniform topmost layer (Table 3, Figure 8).

Very peculiar surface morphology was observed for the star polymer S20-88 with the highest PEO content but the lowest number of arms (Table 1, Figure 2). This polymer formed well-defined dendritic structures at all surface pressures (Figure 9). At low surface pressure, highly branched dendritic morphologies merged into long branched two-dimensional structures oriented transverse to the dipping direction (Figure 9a,b). The height and width of the dendritic structures were very comparable, suggesting that a rise in surface pressure was causing a uniform growth (Table 3). The higher resolution AFM imaging revealed internal domain structures, indicating that the dendrites are assembled by the aggregation of deformed fine circular domains merging into larger aggregates upon compression (Figure 10).

The rise in surface pressure to 5 mN/m resulted in the increased surface coverage from 29% to 49% and domain height growth from 8.1 ± 0.2 nm to 9.5 ± 0.2 nm. Denser and more regular dendritic structures were oriented along the dipping direction at this pressure (Figure 9c,d). The length of the backbones reached tens of microns with the length of branches averaging 2.5 ± 0.5 μm.

At the highest surface pressure, the dense dendritic structure merged into a continuous texture with remnants of the merging and compressed branched structures still evident (Figure 9e,f). The effective thickness rose to 7.3 ± 0.2 nm as the surface coverage exceeded 90%. The surface microroughness of the irregular domains decreased at the highest surface pressure. The overall shapes of the compressed structures followed the initial highly branched morphology with branches squashed in the transverse direction. An interesting feature is the appearance of straight ridges along the former dendrite backbones (Figure 9f). The ridges were 1.5 nm higher than the surrounding monolayer, suggesting the dominating PEO phase thickened as the molecules were compressed along the backbone region. Therefore, the star polymer with the highest PEO content formed dendritic structures at the air–solid interface, indicating that the longer PEO arms were capable of crystallizing at the interface despite star architecture and confinement under PS aggregates.

Suggested Models. Generally, the overall behavior of amphiphilic heteroarm star polymers with a large number of arms follows general trends observed for PEO–PS star copolymers discussed before except for some unexpected features as will be discussed below.¹⁸ From the collected data, we suggest different types of molecular organization for amphiphilic heteroarm star polymers studied here (Figure 1). Cartoons of corresponding structural organizations are presented in Figure 11. First, the molecular ordering of star polymers with low PEO content is controlled by the predominant PS arms, thus forming circular domains aggregated into continuous cylindrical morphology (Figure 5). The shorter PEO chains limit contact between PEO arms of neighboring molecules, thus allowing the PS chains to form continuous one-dimensional structures via lateral aggregation (Figure 11a). An interesting and unique netlike nanostructure was observed for the first time at elevated surface pressure. A 2-fold increase in molecular weight of the PEO arms and the decreasing length of PS arms result in the collapsed cylindrical structure and the formation of densely packed circular micelles (Figure 7). This type of molecular ordering is consistently observed for star polymers with moderate PEO content (Figure 11b). The star polymer with the highest PEO content (88%)

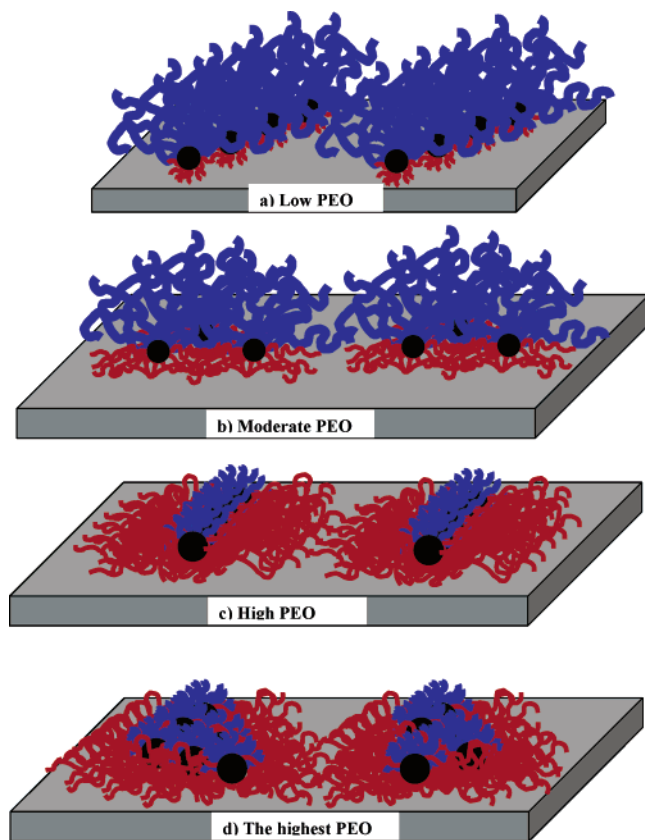


Figure 11. Schematics of molecular ordering in LB monolayers from PEO_nPS_n heteroarm star polymers with low (a), moderate (b), high (c), and the highest (d) PEO content.

forms virtually uniform morphology with an underlying PEO layer covered with PS phase (Figure 11c). A concurrent increase in a number of dissimilar arms attached to a single core (up to 38 for S38-86) prevents microphase separation and the formation of individual circular domains expected for this chemical composition. Instead, upon compression the PEO chains covered segregated PS chains, forming a smooth hydrophilic carpet (Figure 8).

However, reducing the crowding of PS and PEO chains (decreasing the number of arms from 38 to 20) for the S20-88 compound with the highest PEO content promotes in-plane microphase separation with the formation of peculiar dendritic surface morphology. This type of surface morphology is an indication of monolayer growth via diffusion-limited aggregation with preferential directional addition of the components (Figure 11d).⁴⁴ This growth combined with lateral compression eventually leads to the directional growth of PEO monolayer with PS phase vertically segregated in the form of circular domains and 2D dendritic features (Figure 9). Such a unique morphology has never been observed for heteroarm star polymers, but it is known

(44) Sperling, L. H. *Polymeric multicomponent materials: an introduction*; Wiley-Interscience: New York, 1997.

for PEO-containing linear block copolymers. Formation of dendritic-like morphologies of PEO-PS ^{45,46} and PEO-PMPCS ⁴⁷ either from solution or upon isothermal crystallization has been reported. By controlling the crystallization rate, several different patterns ranging from developed dendritic-like to platelets can be formed at isothermal conditions. Therefore, we suggest that PEO crystallization upon solvent evaporation plays a significant role in the formation of interconnected circular domains, which aggregate into larger dendritic interconnected structures.

Recent studies of self-assembly of diblock copolymers suggested that changing experimental condition such as a concentration of deposited polymer solution,^{17b,48} addition of a surfactant,^{41,42} or method of deposition might provide a new tool to control surface morphologies. Therefore, by applying the same methods we may expect the discovery of the new unusual surface morphologies from the heteroarm star polymers.

In conclusion, the ability of PEO_nPS_n star copolymers with different numbers of arms and arm lengths to form ordered domain nanostructures at the air–water and air–solid interfaces was investigated. Monolayers of the star polymers have been transferred onto silicon substrate and examined by AFM. The formation of the peculiar stripe and netlike patterns has been observed for the star polymers with long PS and short PEO chains. These structures have never been observed either in concentrated solutions or in the bulk and seem to be formed only in LB monolayers. Star polymer with 30% PEO and similar PEO and PS chain lengths exhibited a highly ordered 2D assembly of fine circular domains. For the PEO-rich star polymers we observed a strong influence of the number of arms on the morphology of the monolayers. The formation of the very smooth monolayers at a wide range of surface pressures has been examined for the star polymers with 78 and 86% PEO and 38 and 30 arms, respectively. The 20-arm star polymer with the highest PEO content formed peculiar dendritic superstructures (branched textures) upon compression. These structures have never been observed for multiarm PEO-PS star block copolymers. We suggest that the microphase segregation at the air–water interface and PEO crystallization are both triggered by reduced constraints due to the lowered number of arms in the molecules. These processes cause the formation of the spherical or nonspherical core–shell micellar structures followed by spontaneous formation of dendrite patterns.

Acknowledgment. The authors thank M. Goodman for technical assistance. Funding from the National Science Foundation, Grant DMR-0308982, is gratefully acknowledged.

LA060299K

(45) Reiter, G.; Hoerner, P.; Hurtrez, G.; Riess, G.; Sommer, J.-U.; Joanny, J.-F. *J. Surf. Sci. Technol.* **1998**, *14*, 93.

(46) Reiter, G. *J. Polym. Sci., Part B: Polym. Phys.* **2003**, *41*, 1869.

(47) Huang, Y.; Liu, X.-B.; Zhang, H.-L.; Zhu, D.-S.; Sun, Y.-J.; Yan, S.-K.; Wang, J.; Chen, X.-F.; Wan, X.-H.; Chen, E.-Q.; Zhou, Q.-F. *Polymer* **2006**, *47*, 1217.

(48) Hosoi, A. E.; Kogan, D.; Devreux, C. E.; Bernoff, A. J.; Baker, S. M. *Phys. Rev. Lett.* **2005**, *95*, 037801.